Voltage profile, structural prediction, and electronic calculations for $Mg_xMo_6S_8$

K. R. Kganyago* and P. E. Ngoepe†
Materials Modeling Center, School of Physical and Mineral Sciences, University of the North, P/Bag X 1106, Sovenga, 0727, South Africa

C. R. A. Catlow
Davy Faraday Research Laboratory, The Royal Institution of Great Britain, 21 Albemarle Street, London, United Kingdom W1S 4BS
(Received 9 October 2002; published 19 March 2003)

We perform a systematic computational investigation of the new Chevrel phase, $Mg_xMo_6S_8$ for $0 \leqslant x \leqslant 2$, a candidate for a high-energy density cathode in prototype rechargeable magnesium (Mg) battery systems. We conduct our study within the framework of both the local-density-functional theory and the generalized gradient approximation technique. Analysis of the calculated energetics for different magnesium positions and composition suggest a triclinic structure of $Mg_xMo_6S_8$ ($x=1$ and 2). The results compare favorably with experimental data and suggest a charge transfer from Mg to the Mo_6S_8 cluster, having a significant effect on the Mo-Mo bond length.

DOI: 10.1103/PhysRevB.67.104103 PACS number(s): 61.50.Ah, 71.15.−m, 34.70.+e, 82.45.Fk

I. INTRODUCTION

The ternary molybdenum chalcogenides $M_xMo_6X_8$ (M = metal atom, X = S, Se, Te) have been intensively investigated[1–11] because of their high specific density, high electronic conductivity, and high metal diffusion coefficient. Here, we focus our attention on the ternary molybdenum sulphides of formula $M_xMo_6S_8$ ($0<x\leqslant 4$; M = earth-alkaline or earth-alkali metal), which have been widely studied because of their unique physical and chemical properties. Mg intercalated Mo_6S_8 (Refs. 12 and 13) and $Cu_2Mo_6S_8$ (Ref. 14) have been recently reported as possible candidate cathode materials in high-density rechargeable batteries. Electrochemical characteristics of intercalation compounds strongly depend on the morphology of the materials and on their structural perfection.[15] Insertion of magnesium is of particular theoretical and practical interest, because the ion sizes of the monovalent lithium ($Li^+ = 0.76$ Å) and divalent magnesium ($Mg^{2+} = 0.72$ Å) cations are similar. In this paper we investigate the structural and energetic properties of $Mg_xMo_6S_8$ ($0<x\leqslant 2$) based on the reported structure of Chevrel phase compounds $Ni_2Mo_6S_8$ (Refs. 16 and 17) and $Li_xMo_6S_8$ ($0<x\leqslant 4$) (Ref. 10) using the density-functional technique. Electronic properties are then calculated from the newly predicted structures and compared with the reported trends in similar compounds.

A. Structural

As shown in Fig. 1, Chevrel phase structures are made up of blocks of slightly distorted cubes or clusters of Mo_6X_8 units, with eight X atoms at the cube corners and six Mo atoms slightly outside the middle of the cube faces. Most have rhombohedral structures at room temperature and many distort to triclinic structures at low temperature.[18] Mo_6S_8 is rhombohedral with space group $R\bar{3}$ (C_{3i}^2), and lattice parameters $a_R = |\vec{a}| = |\vec{b}| = |\vec{c}| = 6.43$ Å and $\alpha_R = \alpha = \beta = \gamma = 91.34°$.[19] Earlier work on $Li_xMo_6S_8$ (Ref. 20) showed that there are two phases, a rhombohedral phase with an incommensurate lattice distortion, and a triclinic phase for $0<x<1$.

A network of interconnecting channels, parallel to the rhombohedral axes, runs between the Mo_6S_8 clusters which contain the interstitial sites or cavities where the M atoms reside. Cavity 1, which is the largest, has a quasicubic shape and is formed by eight sulfur atoms belonging to eight different Mo_6S_8 units centered at the origin (the position of Mg_O in Fig. 2) of the rhombohedral unit cell with point symmetry $\bar{3}$. Cavity 2, situated at the middle of the rhombohedral axes ($\bar{1}$-point symmetry), has a more irregular cubic shape and is formed by eight sulfurs belonging to four Mo_6S_8 units sharing edges (see Fig. 2). This cavity shares opposite pseudosquared faces with two other cavities, one along the rhombohedral axes. Cavity 3, formed by eight sulfur atoms belonging to two different Mo_6S_8 units, is always empty because of the Mo-S intercluster bond (Fig. 2). For smaller M atoms, α_R is larger and the M atoms are displaced from the $\bar{3}$ axis, and partially occupy one ring of six inner sites inside cavity 1 (site A) and one ring of six outer sites in cavity 2 (site B) per formula unit of Mo_6X_8. When α_R is small, the S($2c$) site is significantly closer to the interstitial site than the S($6f$) site (Fig. 1). The two chalcogens on the $\bar{3}$ axis ($2c$) have the greatest influence on the M-atom site energy because of their closer proximity than the other six chalcogens ($6f$).[21] Two Mo-Mo distances describe the molybdenum cluster: the $[\mathrm{Mo}(1)\text{-}\mathrm{Mo}(1)]_\triangle$ intratriangle and $[\mathrm{Mo}(1)_\triangle\text{-}\mathrm{Mo}(1)_\triangle]$ intertriangle. The first distance concerns two molybdenum atoms belonging to the same triangular plane which is perpendicular to the ternary ($\bar{3}$) axis, while the second distance concerns two adjoining triangular planes in the same cluster [Fig. 1(a)].

The crystal structure of $Mg_xMo_6S_8$ may also be considered as a stacking of Mo_6X_8 clusters. There are 12 potential formal lattice sites for Mg atoms between each set of two blocks, around the unit-cell origin [Figs. 1(b) and 1(c)]. The first ring has sixfold positions (Mg_A) close to the unit-cell

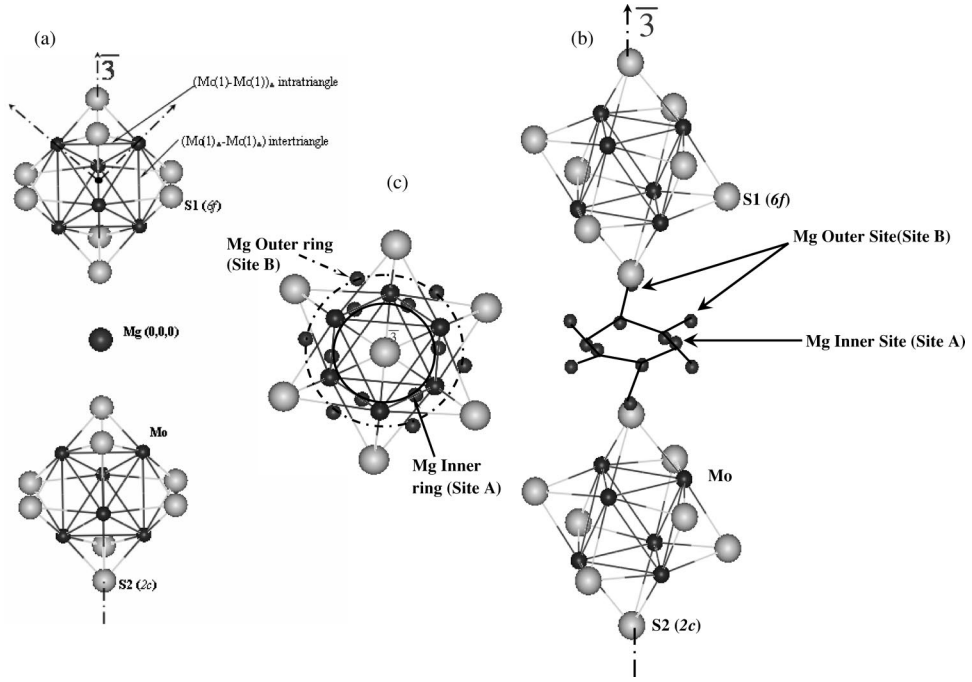

FIG. 1. Basic crystal structure of the $Mg_xMo_6S_8$ ($0 \leqslant x \leqslant 2$) cathodes. (a) Basic atomic arrangements in the rhombohedral Chevrel phase sulphide cluster with (b) two possible Mg positions with a dumbell shape per cavity 2 ($\bar{1}$) and (c) six positions giving a hexagonal or puckered ring per cavity 1 ($\bar{3}$).

origin, forming the inner sites; a second ring with sixfold positions (Mg_B) which forms the outer sites is located around the inner positions. The intercalated metal plays an important role in stabilizing the whole structure. It modifies the distances between the Mo atoms due to charge transfer from the metal atoms to the Mo or S atoms. The maximum charge transfer is predicted to be four electrons per Mo_6S_8 cluster, which results in the maximal insertion of four monovalent Li^+ cations or two bivalent Mg^{2+} cations. Magnesium insertion into $Mg_xMo_3S_4$ takes place in stages corresponding to the formation of new phases. A new intercalation phase differs from the previous one by occupation of different sites [site A or B, see Figs. 1(b) and 1(c)] in the host crystal with a different insertion energy. Mg can be inserted electrochemically up to a stoichiometry of $Mg_xMo_3S_4$ ($x=1$).[12]

Mg insertion into Mo_3S_4 can be understood by reference to the crystal structure of $Li_xMo_3S_4$ ($0<x\leqslant 2$).[10] The ionic model description[3] suggests a maximum uptake formally of two Mg ions into the electron-deficient Mo_6 cluster, which leaves us with two possible vacant sites: the inner Li1 site (substituted by Mg_A) close to the unit-cell origin with the atom coordinates (0.598,0.359,0.381: $\beta=2.9$), and the outer Li2 site (substituted by Mg_B) with the atom coordinates

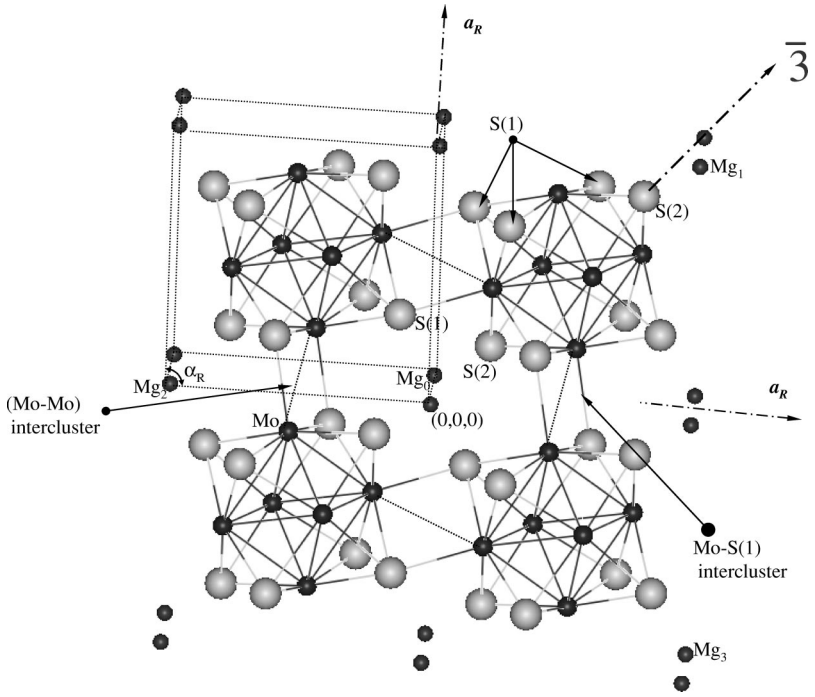

FIG. 2. Crystal structure of the Chevrel phase $Mg_OMo_6S_8$, showing four Mo_6S_8 rhombohedral units (each unit is turned by an angle of about 27° around the ternary axis), the strong (Mo-Mo) intercluster and Mo-S(1) intercluster bonding, and two types of chalcogen atoms [axial S(2) and peripheral S(1)]. Inserted Mg cations are located at position (0,0,0). A hexagonal unit cell can also be defined with Mg_0 being the origin. The vector from Mg_0 to Mg_1 is the c lattice parameter and the vectors from Mg_0 to Mg_2 and Mg_0 to Mg_3 are the a lattice parameters.

(0.156,0.272,0.872:$\beta=1.3$). This configuration leads us to new structures $Mg_AMo_6S_8$ and $Mg_BMo_6S_8$ used in our calculations. A model of the structure of $NiMo_3S_4$ (Refs. 16 and 17) is also considered, using the structure of the stoichiometric compound as a reference and substituting the atomic positions of Ni (0.0144,0.3458,0.9404:$\beta=1.45$) and (0.0558,0.797,0.8192:$\beta=1.89$) by Mg leading to $Mg_{AB}Mo_6S_8$. We also consider Mg occupation of cavity 1 (Mg_O) with the following fractional coordinates (0,0,0), the site normally occupied by large atoms (see Fig. 2).

B. Mg battery system

Magnesium cells are good candidates for high-energy density batteries having advantages over other available rechargeable battery systems, in terms of safety, low cost, and environmental considerations.[12,22] Mg compounds (mostly $MgCO_3$) are highly abundant in the earth and are environmentally benign. In terms of battery applications, the redox potential of the Mg/Mg^{2+} couple is 1-V higher than that of the Li/Li^+ couple.[13] Mg batteries are designed to compete with the environmentally problematic lead-acid and nickel-cadmium batteries for heavy load applications. Realization of fast Mg^{2+} transport in the host is a requirement for a practical cathode material in magnesium cells. Fast Mg^{2+} transport may be expected in Mo_6X_8 compounds because of their large interstitial networks. However, the electrochemistry of metallic magnesium at ambient temperatures is still far from being well understood, and the electrochemical insertion reactions of magnesium have seldom been investigated.[23] Use of magnesium has also been found to be attractive in electrolyte activated reserve batteries for immediate use.[24]

The Chevrel phases are characterized by the valence electron concentration (VEC), i.e., the number of valence electrons in the metal-metal bonded Mo_6 cluster. There would be 20 electrons in the molecular orbitals of the metal-metal bonds of Mo octahedron,[3] and theoretically the host Mo_6X_8 network can accommodate metal ions up to a VEC value as high as 24 electrons per Mo_6 cluster. Addition of the M atoms to the host results in electron transfer, wherein electrons are accepted by the low-lying vacant energy level of the host band (conduction band), which acts as an electron sink.[25] This charge-transfer process is the basis of the cell reaction in which these materials are used as cathodes in solid-state batteries.

C. Theoretical studies of cathode materials

Computer simulations may be used prior to the synthesis of new materials only requiring the crystal structure as input. Such calculations have the potential to point the way to interesting new classes of electrode materials for the next generation of advanced batteries. These calculations have reproduced electrochemical data well, hence they may be used to predict materials with enhanced energy storage abilities. The following are examples of theoretical studies of cathode materials: Reimers and Dahn[26] calculated the appropriate cell voltages for an Li/Li_yAl cell. Aydinol *et al.*[28] calculated the average voltages for $Li/LiMO_2$ and $Li/LiCoX_2$ ($M=$Ti, V, Mn, Co, Ni, Cu, Zn, Al; $X=$O, S, Se) cells. Courtney *et al.*[29] used the *ab initio* pseudopotential plane-wave method and the approximation by Aydinol *et al.*[28] to calculate the average voltage for the anode material tin oxide (in particular, lithium tin, Li_xSn_y). Deiss *et al.*[27] calculated the energy density and cell voltage of $LiC_6/LiMoO_2$ (anode/cathode) and LiC_6/NiO_2 using the average voltage between the fully charged and the discharged states. Benco *et al.*[30] calculated the average voltages of $Li/LiTi_2S_4$ and $Li/LiTi_2O_4$ systems using the full-potential linearized augmented plane-wave method and Doyle *et al.*[31] recently developed a mathematical model to simulate impedance response of the lithium-polymer cell $Li|PEO_{18}LiCF_3SO_3|LiTiS_2$. Braithwaite *et al.*[32–34] used the *ab initio* pseudopotential plane-wave method and the finite difference approximation to calculate the variation of the cell potential of Li/LiV_2O_5, Li/LiV_6O_{13}, and $Li/Li_xCo_yMn_{4-y}O_8$ systems with the degree of discharge. Recently, Koudriachova *et al.*[35,36] also used the *ab initio* pseudopotential plane-wave method to calculate the open cell voltage of $Li/LiTiO_2$. These types of calculations have established the reliability of density-functional theory (DFT) techniques in modeling the energetics of intercalation.

A number of theoretical calculations have been reported for the Chevrel phase compounds,[37–44] though there is considerably less on structural properties and lattice-parameter predictions of Mo_6S_8 and $M_xMo_6S_8$. In this paper we therefore use the DFT method to probe structure and energetic properties of Mg-inserted Chevrel phases with a view to providing insight into their use as cathode materials.

II. METHOD OF CALCULATION

All calculations use the total-energy (E^{tot}) code CASTEP,[45] which employs pseudopotentials to describe electron-ion interactions and represents electronic wave functions using a plane-wave basis set.[46] Calculations were conducted on metallic magnesium (Mg_{metal}), the low-symmetry $R\bar{3}$ structures of $Mg_xMo_6S_8$: Mo_6S_8 ($x=0$) and $Mg_OMo_6S_8$ ($x=1$, Mg at origin); the $P\bar{1}$ structures for ($x=1$) of $Mg_AMo_6S_8$ (Mg in the inner ring) and $Mg_BMo_6S_8$ (Mg in the outer ring); and for ($x=2$) of $Mg_{AB}Mo_6S_8$ (Mg in both site A and site B), $Mg_{2A}Mo_6S_8$ (two Mg's in site A), and $Mg_{2B}Mo_6S_8$ (two Mg's in site B), which involves up to 16 atoms in a unit cell per system. Energy cutoffs of up to 500 eV were used for the expansion of the wave functions and a single point sampling of the Brillouin zone produced converged results.

The total energy is calculated both within the framework of the local-density approximation (LDA), the Perdew and Zunger[47] parametrization of the numerical results of Ceperley and Alder[48] for the exchange-correlation energy, and the nonlocal or gradient-corrected approximations (Perdew-Burke-Ernzerhof[49]) implemented according to the method described by White and Bird.[50] The interactions between the ionic cores and the electrons are described by the Troullier-Martins[51] pseudopotential, the pseudopotential in Kleinman-Bylander[52] form, and the associated Vanderbilt[53]

TABLE I. Calculated and experimental structural parameters for rhombohedral and hexagonal Mo_6S_8 and $Mg_xMo_6S_8$ ($x=1$ and 2).

Compounds	a_R(Å)	α_R(°)	V_R(Å^3)	a_H(Å)	c_H(Å)	V_H(Å^3)	c_H/a_H
Mo_6S_8 (LDA)	6.347	91.39	255.4	9.084	10.722	766.19	1.180
Mo_6S_8 (GGA-PBE)	6.465	91.50	269.9	9.261	10.899	809.78	1.177
Mo_6S_8 [a]	6.432	91.34	265.8	9.201	10.879	797.50	1.182
Mo_6S_8 [b]	6.432	91.34	265.8	9.202	10.877	797.60	1.182
Mo_6S_8 [c]	6.425	91.25	265.0	9.185	10.881	795.10	1.185
Mo_6S_8 [d]	6.424	91.26	264.9	9.184	10.880	794.63	1.185
Mo_6S_8 [e]	6.430	91.31	265.6	9.197	10.879	796.90	1.183
Mo_6S_8 [f]	6.428	91.26	265.4	9.189	10.886	796.21	1.185
$Mg_OMo_6S_8$ (LDA)	6.367	91.52	257.8	9.122	10.730	773.35	1.176
$Mg_OMo_6S_8$ (GGA-PBE)	6.489	92.12	272.7	9.346	10.815	818.23	1.153
Triclinic	a(Å)	b(Å)	c(Å)	α(°)	β(°)	γ(°)	V_T(Å^3)
$Mg_AMo_6S_8$	6.393	6.402	6.385	93.65	93.05	91.62	260.358
$Mg_BMo_6S_8$	6.409	6.386	6.396	93.95	91.03	93.63	260.564
$Mg_{2A}Mo_6S_8$	6.480	6.490	6.557	99.60	90.53	98.04	269.088
$Mg_{AB}Mo_6S_8$	6.505	6.521	6.535	97.27	93.58	92.99	273.936
$Mg_{2B}Mo_6S_8$	6.629	6.515	6.501	94.26	96.78	91.40	277.850

[a]Reference 19.
[b]Reference 55.
[c]Reference 56.
[d]Reference 25.
[e]Reference 57.
[f]Reference 21.

pseudopotential. The earlier pseudopotentials were specifically used for the calculations of electronic properties rather than structural parameters, the latter being well predicted by the Vanderbilt pseudopotential which requires significantly less computational resources.

The pseudowave functions, the smooth part of the charge density, and the potential are represented on a fast-Fourier-transform (FFT) grids of $18\times18\times30$, $40\times40\times40$, and $45\times45\times45$ for Mg_{metal}, Mo_6S_8, and $Mg_xMo_6S_8$ ($0\leqslant x\leqslant 2$), respectively. These minimum FFT grids applied to the exchange-correlation potential $[V_{xc}(G-G')]$ are sufficient for the cutoff energies. The 36 and 6 k points were generated with the Monkhorst-Pack[54] scheme with parameters ($9\times9\times6$) and ($3\times3\times3$) for Mg_{metal} and $Mg_xMo_6S_8$ ($0<x\leqslant 2$), respectively. Each k point in the irreducible Brillouin zone was represented with an equivalent of 6500 to 9600 plane waves. All calculations involve full geometry optimizations of Mg_{metal}, Mo_6S_8, and $Mg_xMo_6S_8$. Geometry optimization at zero pressure as performed with the variable lattice parameter and full relaxation of the internal coordinates. Calculations were considered to be converged when the maximum force on an atom was below 0.01 eV Å^{-1}.

III. RESULTS

We report our results in each of the crystal structures, i.e., $R\bar{3}$ structures of $Mg_xMo_6S_8$: metastable Mo_6S_8 ($x=0$) and $Mg_OMo_6S_8$ ($x=1$); the $P\bar{1}$ structures for ($x=1$) of $Mg_AMo_6S_8$ and $Mg_BMo_6S_8$; and for ($x=2$) of $Mg_{AB}Mo_6S_8$, $Mg_{2A}Mo_6S_8$, and $Mg_{2B}Mo_6S_8$. The cell voltages are calculated from the optimized total energies E^{tot} of the latter structures and that of metallic magnesium (Mg_{metal}). Lastly, details of electronic charge density, including analysis into the effects of intercalation on the electronic structure, are calculated self-consistently for the selected relaxed crystal structures.

A. Structural modeling

Table I gives the calculated structural parameters for both the LDA and generalized-gradient-approximation-Perdew-Burke-Ernzerhof (GGA-PBE) calculations using an ultrasoft representation of the core. The LDA calculations for the rhombohedral structure Mo_6S_8 underestimate the reported experimental[21] parameters well within the expected error: the lattice parameter $a_R=6.347$ Å is less than the experimental values[19,21,25,55–57] which are within the range of 6.424 Å to 6.432 Å while the angle $\alpha_R=91.39°$ is slightly above the experimental range of 91.25° to 91.34°. The same trends follow for the hexagonal Mo_6S_8 structure, with $a_H=9.084$ Å and $c_H=10.722$ Å underestimating the reported experimental parameters which are within the ranges of 9.184 Å to 9.200 Å and 10.877 Å to 10.880 Å, and $V_H=766.190$ Å^3 is below the experimental parameters which range from 794.63 Å^3 to 797.60 Å^3, again well within the expected LDA error.

In contrast, the GGA calculations overestimate lattice parameters in both rhombohedral and hexagonal Mo_6S_8. The lattice parameter $a_R=6.465$ Å and the angle $a_R=91.50°$ are more than experimental values, and the volume V_R

TABLE II. Predicted principal distances and angles of Mo_6S_8 and $Mg_OMo_6S_8$ calculated within both the LDA and GGA compared with experimental distances.

Distances (Å)		Mo_6S_8		$Mg_OMo_6S_8$	
	Experiment [a]	LDA	GGA_{PBE}	LDA	GGA_{PBE}
$(Mo\text{-}Mo)_{\triangle}$	2.698	2.694	2.719	2.683	2.702
$Mo_{\triangle}\text{-}Mo_{\triangle}$	2.862	2.853	2.878	2.754	2.762
$(Mo\text{-}Mo)_{inter}$	3.084	3.006	3.104	3.067	3.190
Mo-S(2)	2.439	2.408	2.418	2.388	2.418
Mo-S(1)	2.426	2.391	2.424	2.393	2.424
S(1)	2.431	2.395	2.424	2.403	2.429
S(1)	2.460	2.417	2.436	2.463	2.486
$[Mo\text{-}S(1)]_{inter}$	2.425	2.378	2.422	2.439	2.496
$S(2)\text{-}S(2)_{diag}$ via Mo_6	6.155	6.067	6.090	5.912	5.973
$S(2)\text{-}S(2)_{diag}$ via origin	4.724	4.655	4.796	4.821	4.825
S(1)-S(2)-S(1) angle (°)	85.94	85.87	86.46	88.54	88.80
Mg-S(2)				2.410	2.413
Mg-Mo(1)				4.503	4.536
Mg-S(1)				5.261	5.286

[a]References 62 and 63.

$=269.928$ Å^3 exceeds experiment[21] by 1.7%. The same trends are noted for the hexagonal Mo_6S_8 structure with $a_H = 9.261$ Å and $c_H = 10.901$ Å, overestimating the reported experimental parameters. Although the GGA slightly overestimates the parameters, the predictions are close to experimental parameters and acceptable for a calculation using the GGA.[58] It has already been shown for a wide range of bulk solids that the GGA tends to overestimate the equilibrium volume V_0 with the least overestimation provided by PBE.[59] The predicted c/a ratio is 1.177 and 1.183 for the GGA and LDA, respectively, similar to the experimental values of 1.182 to 1.185.[19,21,25,55–57]

Since no crystallographic data for $Mg_xMo_6S_8$ have been reported, we infer the position of Mg atoms by analogy with Chevrel compounds suggested by other authors.[10,16,17] The structure of Ritter *et al.*[10] is used, with Mg replacing Li in the $Li_1Mo_6S_8$ structure, where Li exclusively occupies the inner ring (site A), denoted $Mg_AMo_6S_8$. The LDA results suggest a phase transition from a rhombohedral phase to a triclinic phase, an illustration of the very complex structural behavior of the M atoms in the MMo_6S_8 compounds. The existence of triclinic MMo_6X_8 compounds, such as MMo_3S_4 (M=Mg, Fe, Zn, Mn, and Cd), and the low-temperature modification of $Cu_{0.9}Mo_3S_4$ have been reported earlier.[1,4] Yvon *et al.*[3,55] noted a phase transition in the $Cu_xMo_6S_8$ system, with both rings (site A and site B) occupied by Cu ions at high temperature leading to the rhombohedral structure. However, at lower temperatures, the Cu ions are found in positions which are very close to the inner ring (site A) with an empty outer ring leading to a triclinic modification of the structure. The triclinic phase was also observed for $Cu_{1.8}Mo_6S_8$ ($2 \leqslant T_0 \leqslant 270$ K),[60] with two Cu atom positions per unit cell in the interstices, $Fe_2Mo_6S_8$ at $T_0 \cong 400$ K,[4] with Fe atoms occupying equivalent inner rings sites, and $FeMo_6S_8$ at $T_0 \cong 100$ K.[61]

We have also observed a similar phase transition in all the other structures (see Table I) where Mg occupies site A or B for $x=1$, and both sites for $x=2$. The volume increases as the concentration increases from $x=0$ to 2. At $x=2$, the volume is largest when each Mg atom occupies two site B positions ($Mg_{2B}Mo_6S_8$), decreases when the two Mg atoms occupy both site A and site B ($Mg_{AB}Mo_6S_8$), and is smallest for $Mg_{2A}Mo_6S_8$.

Although the origin position, along the $\bar{3}$ symmetry, appears to be too large for small atoms, we nevertheless considered a model with Mg inserted at the origin. The predicted LDA parameters for the rhombohedral $Mg_OMo_6S_8$ with Mg at the origin are $a_R = 6.367$ Å and $\alpha_R = 91.52°$, an increase by 0.3% and 0.1%, respectively, compared to the predicted lattice parameters for Mo_6S_8. The equilibrium volume is predicted to be $V_R = 257.784$ Å^3, an increase of 0.9%. The hexagonal $Mg_OMo_6S_8$ lattice parameters $a_H = 9.122$ Å and $c_H = 10.73$ Å predicted a small increase in the basal plane and almost no variation along the c axis, probably confirming the relatively large size of cavity 1 for Mg. Increasing a_H caused the c/a ratio to decrease by 0.3%, a trend observed for $LiMo_6S_8$,[10] where $c/a = 1.161$. The GGA results also predicted increments of 0.36%, 0.67%, and 1% for a_R, α_R, and V_R, respectively, in comparison with the predicted lattice parameters for Mo_6S_8 with a notable decrease in the c_H lattice parameter.

1. Interatomic and intercluster distances and their variation with Mg position

Table II shows the interatomic and intercluster distances of Mo_6S_8 and their variation with Mg position. We predicted, well within the LDA error margin, the reported experimental internal parameters for Mo_6S_8, a metastable compound only obtained by deintercalation using a ternary compound such as $Cu_2Mo_6S_8$ or $Ni_2Mo_6S_8$.[62] Notably the GGA overesti-

TABLE III. Calculated interatomic distances for rhombohedral $Mg_OMo_6S_8$ and triclinic $Mg_AMo_6S_8$ compared with $LiMo_6S_8$.

Distances (Å)	$Mg_OMo_6S_8$	$Mg_AMo_6S_8$	$LiMo_6S_8$ [a]
$(Mo\text{-}Mo)_{\triangle}$	2.683	2.682	2.688
$Mo_{\triangle}\text{-}Mo_{\triangle}$	2.754	2.741	2.821
$(Mo\text{-}Mo)_{inter}$	3.067	3.117	3.133
Mo-S(2)	2.388	2.417	2.429
Mo-S(1)	2.393	2.389	2.402
S(1)	2.403	2.413	2.448
S(1)	2.463	2.453	2.455
$[Mo\text{-}S(1)]_{inter}$	2.439	2.454	2.474
$S(2)\text{-}S(2)_{diag}$ via Mo_6	5.912	5.969	
M-S(2)	2.401	4.702	2.005
S(2)		3.851	2.985
M-S(1)	5.261	2.543	2.407
S(1)		5.587	2.888
S(1)			2.295
M-Mo(1)	4.503	3.453	3.608

[a]Reference 10.

mated the internal parameters within a small margin with the exception of the Mo-S(1) and Mo-S(2) distances which are underestimated but are very close to the experimental values. Mg insertion introduces distortion of the Mo_6S_8 structure in the $Mg_OMo_6S_8$ compound. The LDA calculated distances generally increase upon inserting Mg in Mo_6S_8. The Mo-S(2) distance of 2.408 Å increases by 0.6% and the intercluster Mo-S(1) distance of 2.378 Å increases by 2.5%. The Mo-S(1) distances of 2.391 Å, 2.395 Å, and 2.417 Å, where S(1) is one of the eight triply bridging sulphur atoms capping each Mo octahedron face (see Fig. 2), increase by (1.4 −1.7)%. The S(1)-S(2)-S(1) angle predicted by both the LDA and GGA predicts an increase from 85.87° to 88.54° and 86.46° to 89.1°, respectively.

It is known that intercalation of Cu in $Cu_xMo_6S_8$ leads, via parallel electron transfer, to reduced Mo-Mo distances.[55] LDA and GGA predictions show a decrease in both the $[Mo(1)\text{-}Mo(1)]_{\triangle}$ intratriangle and the $Mo(1)_{\triangle}\text{-}Mo(1)_{\triangle}$ intertriangle distances. A notable exception occurs with the first distance between two molybdenum atoms belonging to the same triangular plane, perpendicular to the ternary $(\overline{3})$ axis, which decreases by ~0.5%, while the second distance between two adjoining triangular planes in the same cluster decreases by ~3%. The distance between Mg and Mo of 4.503 Å is large enough to exclude direct bonding; hence the cluster Mo_6S_8 can be regarded as a pseudoatom acting as an electron acceptor.

If one compares analogous distances between the binary Mo_6S_8 and $Mg_AMo_6S_8$ (see Table III), the Mo-Mo distances decrease by (0.5−1)%. This decrease corresponds to an anisotropic contraction of the Mo_6 octahedron. The Mo cluster of the rhombohedral compounds forms an elongated octahedron of symmetry $\overline{3}$, while the Mo octahedron of the present structure is triclinically distorted. The S(2)-S(2) diagonal distance via the Mo_6 cluster decreases by 1.6%. The bond and intercluster contact distances of the triclinic $Mg_AMo_6S_8$ modification have small, though varying, differences from those of the rhombohedral $Mg_OMo_6S_8$. The cell volume at the rhombohedral-to-triclinic phase transition increases by 2.6 $Å^3$.

Table III shows the interatomic distances for rhombohedral $Mg_OMo_6S_8$ and triclinic $Mg_AMo_6S_8$ compared with $LiMo_6S_8$. Our results are in good correspondence with the results of structural investigation reported on $Li_xMo_6S_8$.[10] All interatomic distances have values that are typical for Mo sulphides: Mo-S, 2.35 Å (MoS_2) and 2.36−2.57 Å (Mo_2S_3); S-S, 3.31−3.55 Å (Mo_3S_4);[55] and Mo-S, 2.46 Å [$LiMoS_2$ (Ref. 58) and MMo_2S_4, M=Fe or Co (Ref. 64)]. The Mo-Mo distances in pure metal are 2.72 Å and 2.85 Å in Mo_2S_3, 2.91 Å in $LiMoS_2$,[58] and 2.89 Å and 2.90 Å in MMo_2S_4: M=Fe, Co.[64] The Mg sulphide interatomic distances also correspond well with Mg-S, 2.011 Å in $MgS_2O_3\cdot 6H_2O$ (Ref. 65), for Mg-S(2). The cell constant for the cubic (rocksalt) structure of MgS has been reported as 5.201 Å, 5.2036 Å, 5.1913 Å and 5.2018 Å (Ref. 66) and for the zincblende phase at about 5.66 Å,[67] such that the Mg-S bond distance is ~2.6 Å and 4.6 Å, respectively, the latter comparing closely with the Mg-S(1) distance.

B. Energies and cell voltages

The electrochemical topotactic redox reactions can be summarized as follows:

$$x\mathrm{Mg}^{n+} + nxe^- + \mathrm{Mo_6S_8} \Leftrightarrow (\mathrm{Mg}^{n+})_x[\mathrm{Mo_6S_8}]^{nx-}.$$

The negative excess charge in $[Mo_6S_8]^{2x-}$ is compensated by the simultaneous uptake of the mobile Mg^{2+} cation, which occupies empty sites in the lattice channels. Table IV reports the calculated total energies E^{tot} for the host Chevrel phase Mo_6S_8; metallic magnesium Mg_{metal}; and the intercalate compounds $Mg_OMo_6S_8$, $Mg_AMo_6S_8$, $Mg_BMo_6S_8$, and $Mg_{AB}Mo_6S_8$. From these we calculate the value of $\triangle E$ for the intercalation reaction which is given by

$$\triangle E = E^{tot}_{\mathrm{Mg_xMo_6S_8}} - (E^{tot}_{\mathrm{Mo_6S_8}} + E^{tot}_{\mathrm{Mg}_{metal}}). \qquad (1)$$

Comparison of the energies from Table IV clearly shows that Mg preferential positions are the two sixfold crystallographic positions (sites A and B), away from the origin position such as in $Mg_OMo_6S_8$. These positions are indeed ex-

TABLE IV. Calculated E^{tot} for Mo_6S_8, Mg_{metal}, $MgMo_6S_8$, $Mg_AMo_6S_8$, $Mg_BMo_6S_8$, and $Mg_{AB}Mo_6S_8$ systems.

	Total energy, E^{tot} (eV)	$\triangle E$(eV)
Mg_{metal}	−1947.012	
Mo_6S_8	−13851.641	
$Mg_OMo_6S_8$	−14827.188	−2.03
$Mg_AMo_6S_8$	−14827.366	−2.22
$Mg_BMo_6S_8$	−14827.374	−2.23
$Mg_{2A}Mo_6S_8$	−15802.625	−1.99
$Mg_{AB}Mo_6S_8$	−15802.458	−1.91
$Mg_{2B}Mo_6S_8$	−15802.450	−1.90

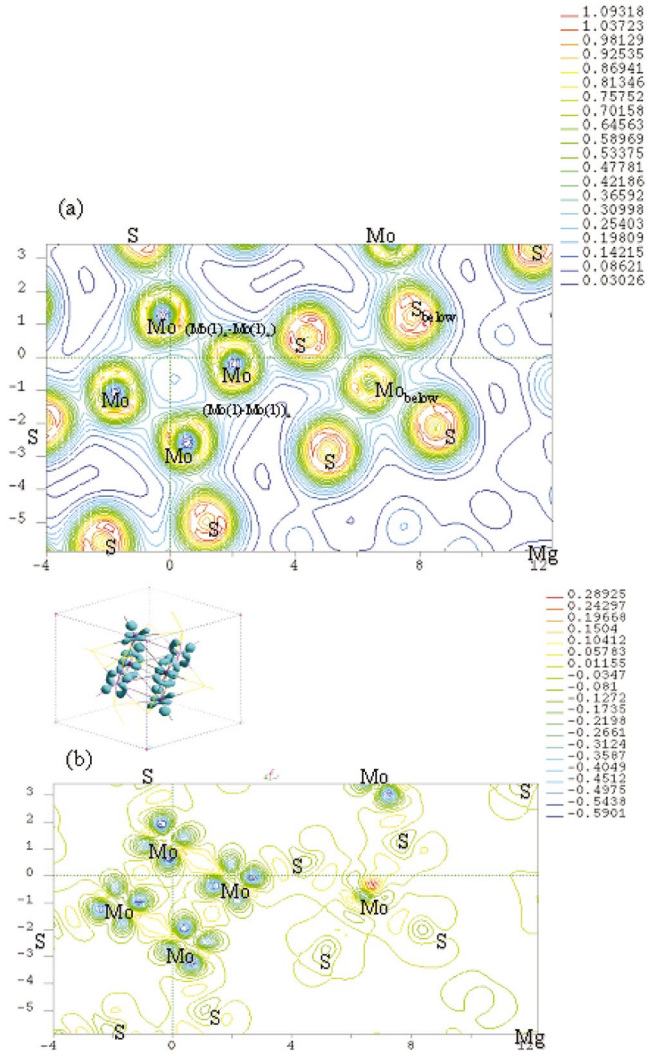

FIG. 3. (Color) Contour plot of (a) the total valence electron pseudocharge density of $Mg_OMo_6S_8$ and (b) the pseudocharge difference of the Mo_6 cluster and the S_8 and Mg in the plane that spans the $Mo(1)_{\triangle}$-$Mo(1)_{\triangle}$ and $[Mo(1)\text{-}Mo(1)_{\triangle}]$ distances. The color coding is dark blue to red/magenta for increasing density. The contour values range from 0.03 to 1.09 and -0.59 to 0.28 $e/\text{Å}^3$, respectively. The isodensity (inset) is plotted at -0.15 within a range of -0.33 to 0.13 $e/\text{Å}^3$.

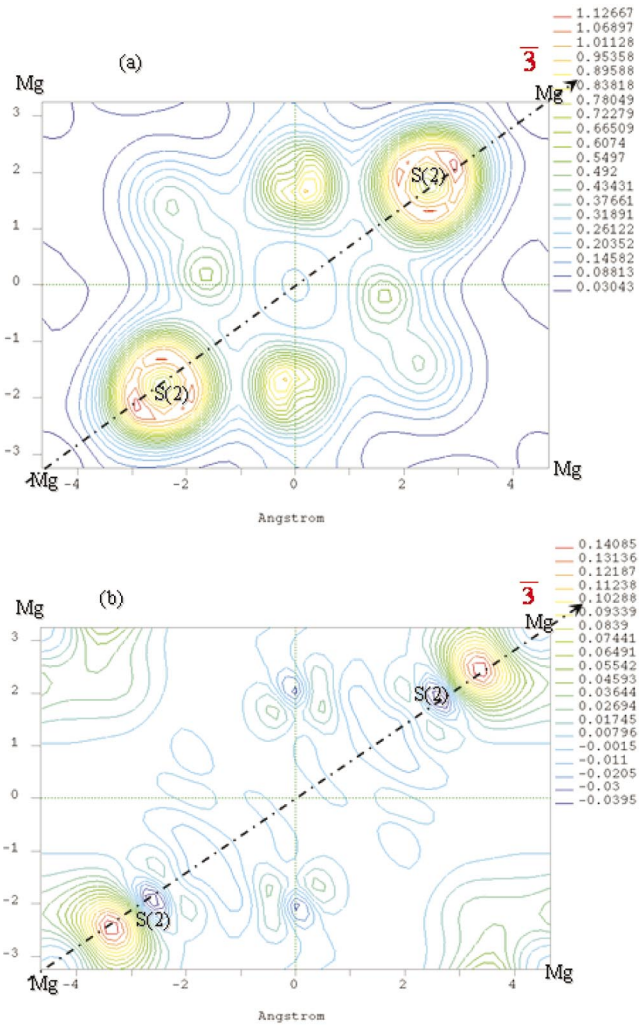

FIG. 4. (Color) The charge-density plot showing a slice of (a) the pseudocharge density and (b) pseudocharge-density difference for $Mg_OMo_6S_8$ along the plane that includes the S(2) sulfur and Mg at the origin parallel to the $\bar{3}$ axis. The color coding is dark blue to red/magenta for increasing density. The density varies between 0.03 to 1.12 and -0.03 to 0.14 $e/\text{Å}^3$, respectively.

pected distributions for small ions in the Chevrel phases. When comparing the geometrical arrangement of inner and outer Mg sites from the $Mg_1Mo_6S_8$ transition to $Mg_2Mo_6S_8$, noticeable changes in the site energy are observed. The occupation of the inner Mg_A site, for $x=2$, close to the unit-cell origin seems preferable while for $x=1$, site A or B will be equally occupied. Using the values given in Table IV, we obtain an average value of about -2.00 eV for $\triangle E_{LDA}$ for $x=1$. This result can be compared with experimental data of Aurbach *et al.*,[12] who report a value of ~ 2 V. The agreement between theory and experiment is gratifying.

C. Charge density

In the $M_x^{n+}Mo_6X_8$ Chevrel phases, a charge transfer of $(nx)e^-/Mo_6$ is thought to occur at the Mo_6 cluster.[3] Hence for $Mg_2Mo_6S_8$, the maximum charge transfer predicted is equivalent to $4e^-/Mo_6S_8$. The calculated total and difference of the (between crystal and atomic superpositions) valence electron pseudoion charge density of $Mg_OMo_6S_8$ ($x=1$), in the plane that spans the $Mo(1)_{\triangle}$-$Mo(1)_{\triangle}$ and $[Mo(1)\text{-}Mo(1)]_{\triangle}$ distances parallel to the ternary $(\bar{3})$ axis, are shown in Figs. 3(a) and 3(b). The Mo atom deformation from a spherical shape is evident in the difference density. There is a four-lobe shape of the charge distribution around each Mo atom visible in the plane and an extra two lobes perpendicular to the plane in the isodensity plot (inset), resembling *d*-type orbitals. There is a notable gain of electrons between both the Mo atoms and Mo-S atoms, showing covalent bonding, with the charges around the S atoms resembling the *p*-type orbitals.

In order to study the more interesting effects of charge

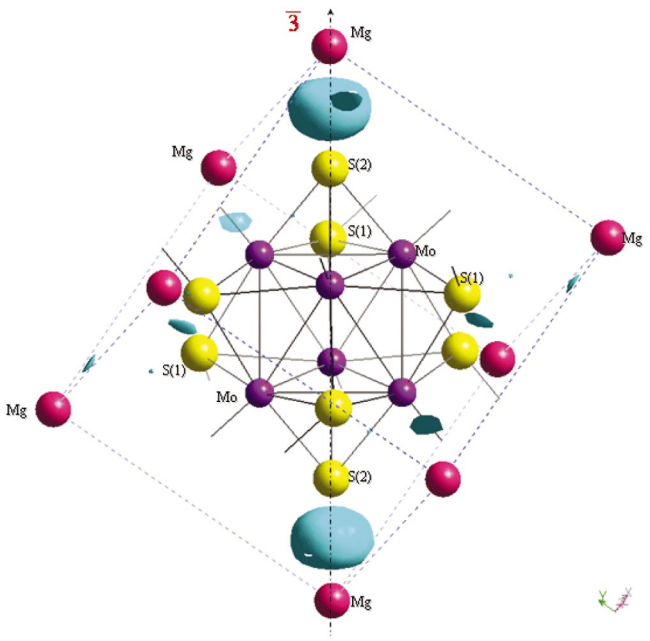

FIG. 5. (Color) The charge-density plot showing a isosurface of the total charge-density difference of $Mg_OMo_6S_8$ and Mo_6S_8 along the plane that includes the S(2) sulfur and Mg at the origin parallel to the $\bar{3}$ axis. The color coding for the isosurface is light blue, plotted at 0.06 within a range of -0.09 to 0.15 $e/Å^3$.

transfer and polarization, we compared the density of $Mg_OMo_6S_8$ and Mo_6S_8. The total electron difference ($Mg_OMo_6S_8$-Mo_6S_8) is shown in Fig. 3(b) also in the plane that spans the $Mo(1)_\triangle$-$Mo(1)_\triangle$ and $[Mo(1)_\triangle$-$Mo(1)_\triangle]$ distances. The density varies between -0.03 and 0.07 $e/Å^3$.

Figure 4(a) shows the total-valence-charge electron density of $Mg_OMo_6S_8$ along the plane that includes the S(2) and Mg at the origin parallel to the $\bar{3}$ axis. The density varies between 0.03 and 1.13 $e/Å^3$. There is a clear high charge concentration around the S(2) atoms with almost no charge around the Mg, hence signifying a loss of charge from Mg. The total electron difference ($Mg_OMo_6S_8$-Mo_6S_8) is shown in Fig. 4(b). A peak of 0.14 $e/Å^3$ is found at the midpoint between S(2) and Mg atoms. Although the charge transfer is consistent with the formula $Mg_2^{2+}[Mo_6^{2+}S_8^{2-}]^{4-}$, there is a substantial measure of charge transfer to the S(2) sulphur atom.

The isosurface in Fig. 5 is plotted at 0.06 within a range of -0.09 to 0.15 $e/Å^3$. There is a quantitative charge transfer evident from the Mg site to the host lattice, confirming the idea that Mg is characterized by ionic bonding in this compound. The number of the valence electrons should increase due to easy redistribution of electronic charge on each element (Mo or S).

Figure 6 shows the contour plot of the pseudocharge difference of the Mo_6 cluster and S_8 and Mg in a plane parallel to the $[Mo\text{-}S(1)]_{inter}$ and Mo-S(1) distances. The four lobes around the Mo atoms resembling the *d*-type orbitals are visible. The formation of the intercluster bond is by $3p$ [S(1)] and $4d$ (Mo) orbitals. A smeared minimum is observed behind the S(1) atoms and extends towards the Mo atom.

IV. CONCLUSION

Lattice parameters of Mo_6S_8 have been calculated within the LDA and GGA with a good reproduction of experimental results. We have studied the insertion of Mg into different positions in Mo_6S_8. The Mg ions prefer to occupy the sixfold crystallographic sites, (site A or B) to the origin site, and the final structure adopts a triclinic phase. Calculated cell voltages are in good agreement with experiment. Charge transfer from the Mg atom to the cluster is evident, with the transferred density being distributed on both Mo and S atoms.

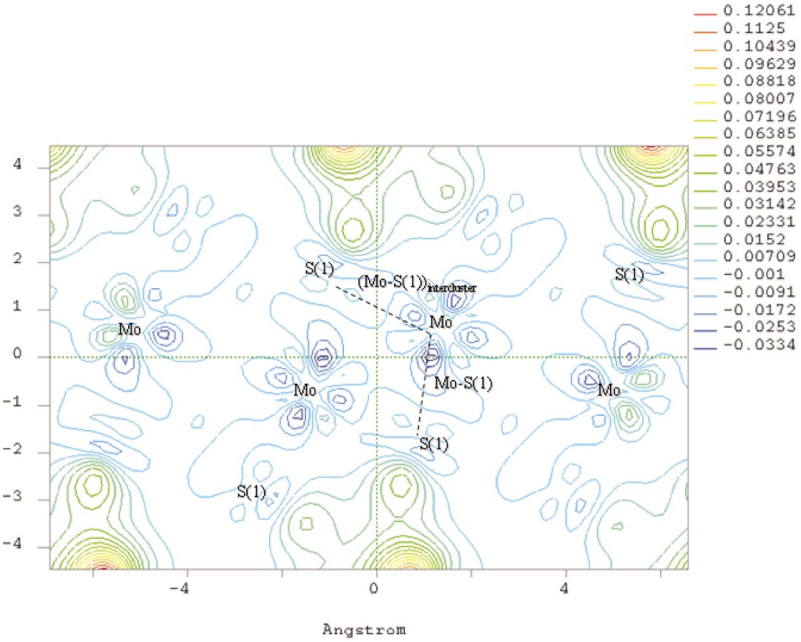

FIG. 6. (Color) The charge-density difference plot of the total charge density of $Mg_OMo_6S_8$ and Mo_6S_8 in a plane parallel to the $[Mo\text{-}S(1)]_{inter}$ and Mo-S(1) distances.

ACKNOWLEDGMENTS

We would like to acknowledge the National Research Foundation (South Africa) and Royal Society [United Kingdom (UK)] for financial support of this work. We are also grateful to the Materials Modeling Center for the availability of computational facilities at the University of the North, and to EPSRC for funding the computing facilities at the Royal Institution (UK).

*Electronic address: khomotso@unorth.ac.za

†Also at Manufacturing and Materials Technology, Council for the Scientific and Industrial Research, Pretoria, 0001, South Africa.

[1] R. Chevrel, M. Sergent, and J. Prigent, J. Solid State Chem. **3**, 515 (1971).

[2] R. Schöllhorn, M. Kümpers, and J. O. Besenhard, Mater. Res. Bull. **12**, 781 (1977).

[3] K. Yvon, in *Current Topics in Materials Science*, edited by E. Kaldis (North-Holland, Amsterdam, 1979), Vol. 3, p. 53.

[4] K. Yvon, R. Chevrel, and M. Sergent, Acta Crystallogr., Sect. B: Struct. Crystallogr. Cryst. Chem. **36**, 685 (1980), and references therein.

[5] J. M. Tarascon, F. J. Disalvo, D. Murphy, G. W. Hull, E. A. Rietman, and J. V. Waszczak, J. Solid State Chem. **54**, 204 (1984).

[6] W. R. McKinnon and J. R. Dahn, Solid State Commun. **52**, 245 (1984).

[7] P. J. Mulhern and R. R. Haering, Can. J. Phys. **62**, 527 (1984).

[8] Y. Takeda, R. Kanno, M. Noda, and O. Yamamoto, Mater. Res. Bull. **20**, 71 (1985).

[9] T. Uchida, K. Watanabe, M. Wakihara, and M. Taniguchi, Chem. Lett. **8**, 1095 (1985).

[10] C. Ritter, E. Gocke, C. Fischer, and R. Schöllhorn, Mater. Res. Bull. **27**, 1217 (1992).

[11] L. Guohua, H. Ikuta, T. Uchida, and M. Wakihara, J. Power Sources **54**, 519 (1995).

[12] D. Aurbach, Z. Lu, A. Schechter, Y. Gofer, H. Gizbar, R. Turgeman, Y. Cohen, M. Moshkovich, and E. Levi, Nature (London) **407**, 724 (2000).

[13] D. Aurbach, Y. Gofer, Z. Lu, A. Schechter, O. Chusid, H. Gizbar, Y. Cohen, V. Ashkenazi, M. Moshkovich, R. Turgeman, and E. Levi, J. Power Sources **97**, 28 (2001).

[14] E. Levi, Y. Gofer, Y. Vestfreed, E. Lancry, and D. Aurbach, Chem. Mater. **14**, 2767 (2002).

[15] M. Winter, J. O. Besenhard, M. E. Spahr, and P. Novak, Adv. Mater. **10**, 725 (1998).

[16] J. Guillevic, O. Bars, and D. Grandjean, J. Solid State Chem. **7**, 158 (1973).

[17] J. Guillevic, O. Bars, and D. Grandjean, Acta Crystallogr., Sect. B: Struct. Crystallogr. Cryst. Chem. **32**, 1338 (1976).

[18] J. R. Dahn, W. R. McKinnon, and S. T. Coleman, Phys. Rev. B **31**, 484 (1985).

[19] M. Sergent and R. Chevrel, J. Solid State Chem. **6**, 433 (1973).

[20] W. R. McKinnon and J. R. Dahn, Phys. Rev. B **31**, 3084 (1985).

[21] L. S. Selwyn, W. R. McKinnon, J. R. Dahn, and Y. Le Page, Phys. Rev. B **33**, 6405 (1986).

[22] K. Makino, Y. Katayama, T. Miura, and T. Kishi, J. Power Sources **99**, 66 (2001).

[23] P. Novák, W. Scheifele, and O. Haas, J. Power Sources **54**, 479 (1995).

[24] G. Kumar, A. Sivashanmugam, N. Muniyandi, S. K. Dhawan, and D. C. Trivedi, Synth. Met. **80**, 279 (1996).

[25] C. Fischer, E. Gocke, U. Stege, and R. Schöllhorn, J. Solid State Chem. **102**, 54 (1993).

[26] J. N. Reimers and J. R. Dahn, Phys. Rev. B **47**, 2995 (1993).

[27] E. Deiss, A. Wokaun, J. L. Barass, C. Daul, and P. Dufek, J. Electrochem. Soc. **144**, 3877 (1997).

[28] M. K. Aydinol, A. F. Kohan, G. Ceder, K. Cho, and J. Joannopoulos, Phys. Rev. B **56**, 1354 (1997).

[29] I. A. Courtney, J. S. Tse, Ou Mao, J. Hafner, and J. R. Dahn, Phys. Rev. B **58**, 15 583 (1998).

[30] L. Benco, J.-L. Barras, M. Atanasov, and C. Daul, J. Solid State Chem. **145**, 503 (1999).

[31] M. Doyle, J. P. Meyers, and J. Newman, J. Electrochem. Soc. **147**, 99 (2000).

[32] J. S. Braithwaite, C. R. A. Catlow, J. H. Harding, and J. D. Gale, Phys. Chem. Chem. Phys. **2**, 3841 (2000).

[33] J. S. Braithwaite, C. R. A. Catlow, J. D. Gale, J. H. Harding, and P. E. Ngoepe, J. Mater. Chem. **10**, 239 (2000).

[34] J. S. Braithwaite, C. R. A. Catlow, J. H. Harding, and J. D. Gale, Phys. Chem. Chem. Phys. **3**, 3841 (2001).

[35] M. V. Koudriachova, N. M. Harrison, and S. W. de Leeuw, Phys. Rev. Lett. **86**, 1275 (2001).

[36] M. V. Koudriachova, N. M. Harrison, and S. W. de Leeuw, Phys. Rev. B **65**, 235423 (2002).

[37] L. F. Mattheiss and C. Y. Fong, Phys. Rev. B **15**, 1760 (1977).

[38] D. W. Bullett, Phys. Rev. Lett. **39**, 664 (1977).

[39] O. K. Andersen, W. Klose, and H. Nohl, Phys. Rev. B **17**, 1209 (1978).

[40] T. Jarlborg and A. J. Freeman, Phys. Rev. Lett. **44**, 178 (1980).

[41] H. Nohl, W. Klose, and O. K. Andersen, in *Superconductivity in Ternary Compounds I*, edited by Ø. Fischer and M. B. Maple, Vol. 32 of *Topics in Current Physics* (Springer, Berlin, 1982), pp. 165–221.

[42] R. W. Nunes, I. I. Mazin, and D. J. Singh, Phys. Rev. B **59**, 7969 (1999).

[43] C. Roche, R. Chevrel, A. Jenny, P. Pecheur, H. Scherrer, and S. Scherrer, Phys. Rev. B **60**, 16 442 (1999).

[44] K. Kobayashi, A. Fujimori, T. Ohtani, I. Dasgupta, O. Jepsen, and O. K. Andersen, Phys. Rev. B **63**, 195109 (2001).

[45] V. Milman, B. Winkler, J. A. White, C. J. Pickard, M. C. Payne, E. V. Akhmatskaya, and R. H. Nobes, Int. J. Quantum Chem. **77**, 895 (2000).

[46] M. C. Payne, M. P. Teter, D. C. Allan, and J. D. Joannopoulos, Rev. Mod. Phys. **64**, 1045 (1992), and references therein.

[47] J. P. Perdew and A. Zunger, Phys. Rev. B **23**, 5048 (1981).

[48] D. M. Ceperley and B. J. Alder, Phys. Rev. Lett. **45**, 566 (1980).

[49] J. P. Perdew, K. Burke, and M. Ernzerhof, Phys. Rev. Lett. **77**, 3865 (1996).

[50] J. A. White and D. M. Bird, Phys. Rev. B **50**, 4954 (1994).

[51] N. Troullier and J. L. Martins, Phys. Rev. B **43**, 1993 (1991).

[52] L. Kleinman and D. M. Bylander, Phys. Rev. Lett. **48**, 1425 (1982).

[53] D. Vanderbilt, Phys. Rev. B **41**, 7892 (1990).

[54] H. J. Monkhorst and J. D. Pack, Phys. Rev. B **13**, 5188 (1976).
[55] K. Yvon, A. Paoli, R. Flükiger, and R. Chevrel, Acta Crystallogr., Sect. B: Struct. Crystallogr. Cryst. Chem. **33**, 3066 (1977).
[56] J. M. Tarascon, F. J. Di Salvo, J. V. Waszczak, and G. W. Hull, Jr., Phys. Rev. B **31**, 1012 (1985); *ibid.* **31**, 8280(E) (1985).
[57] H. Hinode, Y. Ohira, and M. Wakihara, Thermochim. Acta **282**, 331 (1996).
[58] X. Rocquefelte, F. Boucher, P. Gressier, G. Ouvrard, P. Blaha, and K. Schwarz, Phys. Rev. B **62**, 2397 (2000).
[59] S. Kurth, J. P. Perdew, and P. Blaha, Int. J. Quantum Chem. **75**, 889 (1999).
[60] R. Baillif, K. Yvon, R. Flükiger, and J. Muller, J. Low Temp. Phys. **37**, 231 (1979).
[61] J. M. Friedt, C. W. Kimball, A. T. Aldred, B. D. Dunlap, F. Y. Fradin, and G. K. Shenoy, Phys. Rev. B **29**, 3863 (1984).
[62] R. Chevrel and M. Sergent, in *Topics in Current Physics*, edited by Ø. Fischer and M. B. Maple (Springer-Verlag, Berlin, 1982), Vol. 32, pp. 25.
[63] R. Chevrel, M. Sergent, and J. Prigent, Mater. Res. Bull. **9**, 1487 (1974).
[64] J. Guillevic, J. Y. Le Marouille, and D. Grandjean, Acta Crystallogr., Sect. B: Struct. Crystallogr. Cryst. Chem. **30**, 111 (1974).
[65] Y. Elerman, H. Fuess, and W. Joswig, Acta Crystallogr., Sect. B: Struct. Crystallogr. Cryst. Chem. **38**, 1799 (1982).
[66] Y. Takeuchi, S. Sasaki, K. A. Bente, and K. Tsukimura, Acta Crystallogr., Sect. B: Struct. Crystallogr. Cryst. Chem. **49**, 780 (1993), and references therein.
[67] L. Konczewicz, P. Bigenwald, T. Cloitre, M. Chibane, R. Ricou, P. Testud, A. Briot, and R. L. Aulombard, J. Cryst. Growth **159**, 117 (1996).